

MGAug: Multimodal Geometric Augmentation in Latent Spaces of Image Deformations

Tonmoy Hossain¹, Jian Wang³, Miaomiao Zhang^{1,2}

¹Department of Computer Science, University of Virginia

²Department of Electrical and Computer Engineering, University of Virginia

³Department of Radiology, Boston Children’s Hospital, Harvard Medical School

Abstract

Geometric transformations have been widely used to augment the size of training images. Existing methods often assume a unimodal distribution of the underlying transformations between images, which limits their power when data with multimodal distributions occur. In this paper, we propose a novel model, *Multimodal Geometric Augmentation* (MGAug), that for the first time generates augmenting transformations in a multimodal latent space of geometric deformations. To achieve this, we first develop a deep network that embeds the learning of latent geometric spaces of diffeomorphic transformations (a.k.a. diffeomorphisms) in a variational autoencoder (VAE). A mixture of multivariate Gaussians is formulated in the tangent space of diffeomorphisms and serves as a prior to approximate the hidden distribution of image transformations. We then augment the original training dataset by deforming images using randomly sampled transformations from the learned multimodal latent space of VAE. To validate the efficiency of our model, we jointly learn the augmentation strategy with two distinct domain-specific tasks: multi-class classification on 2D synthetic datasets and segmentation on real 3D brain magnetic resonance images (MRIs). We also compare MGAug with state-of-the-art transformation-based image augmentation algorithms. Experimental results show that our proposed approach outperforms all baselines by significantly improved prediction accuracy. Our code is publicly available at <https://github.com/tonmoy-hossain/MGAug>.

Introduction

Recent advances in deep learning (DL) have led to remarkable progress in image analysis tasks, including but not limited to image classification (Krizhevsky, Sutskever, and Hinton 2017; Wang and Zhang 2022), segmentation (Hossain et al. 2019; Chen et al. 2021), object detection (Kim and Pavlovic 2016; Pang et al. 2019), and 3D reconstruction (Jayakumar, Hossain, and Zhang 2023). The literature has shown that deep neural networks (DNNs) are most powerful when trained on vast amounts of manually labeled data. Unfortunately, many image applications have relatively small annotated datasets available, due to privacy concerns, regulations, costs, and incidents of disease. The DNNs, in such cases, tend to overfit due to their poor generalizations to large data variances. Data augmentation (DA) is a simple,

yet efficient and commonly used strategy to overcome this issue by synthesizing more training examples to artificially increase the dataset (Cubuk et al. 2019; Zhao et al. 2019; Zoph et al. 2020; Shen et al. 2020). It is often employed as a preprocessing step applied to the training data to expose the DNNs to various types of approximated invariance; hence reducing the problem of overfitting. In the image domain, common augmentation strategies include adding variations to image intensities (Gao et al. 2021), or deforming the image by randomly generated geometric transformations (i.e., translation, rotation, or scaling) (Moreno-Barea et al. 2018). This paper focuses on DA, particularly in geometric spaces.

In practice, DA is usually a manual process where a human specifies a set of affine or deformable transformations believed to make DL models invariant (Hendrycks et al. 2019; Yun et al. 2019). However, such methods can pose a high risk of producing unrealistic or implausible variations of the image. For example, rotating an image 180 degrees makes sense for natural images, but produces ambiguities on digital numbers (i.e., the digits ‘6’ and ‘9’). In medical domain, randomly generated deformations may transform images from a healthy to a diseased group. To alleviate this issue, researchers have developed a group of automatic DA methods that learn an optimal augmenting policy from the data itself (Cubuk et al. 2019; Lim et al. 2019; Zoph et al. 2020; Araslanov and Roth 2021; Muralikrishnan et al. 2022). One approach is to learn a generator via generative adversarial networks (GANs) to synthesize data from scratch (Mirza and Osindero 2014; Chen et al. 2022). However, these models are difficult to train due to the high complexity of largely unknown parameter spaces (Jaderberg et al. 2015). Despite showing encouraging results on relatively easy datasets (e.g., 28² MNIST), they do not appear to be applicable to more complex datasets with large structural and geometric variances. Another common approach is to learn a probabilistic distribution of a set of deformable transformations derived from the training images (Hauberg et al. 2016; Krebs et al. 2019; Dalca et al. 2019; Zhao et al. 2019; Olut et al. 2020; Shen et al. 2020). Most importantly, these methods assume a unimodal distribution of the underlying transformations between images. They do not provide an appropriate way to learn the full space of geometric transformations among the training data. This greatly limits their power when multimodal data (e.g., time-series/longitudinal

images, or images of multiple sub-populations) occurs.

In this paper, we present a novel model, MGAug, that for the first time learns augmenting transformations in a *multimodal latent space of geometric deformations*. In contrast to existing approaches limited to data with unimodal distributions, our MGAug features the main advantages of

- (i) Generalizing the automatic DA process into a geometric space that allows hidden transformations with multiple modes.
- (ii) Developing a new generative model that learns the latent distribution of augmented transformations via a mixture of multivariate Gaussians defined as a prior in the tangent space of diffeomorphisms.
- (iii) Improving the quality of augmented samples from learned knowledge of training data itself with intra-group constraints.

We demonstrate the effectiveness of our proposed model in two distinct domain-specific tasks: multi-class classification and segmentation on both 2D synthetic data and real 3D brain magnetic resonance images (MRIs), respectively. We also compare MGAug with the state-of-the-art transformation-based augmentation algorithms (Olut et al. 2020; Dalca et al. 2019). Experimental results show that our method outperforms all baseline algorithms by significantly improved prediction accuracy.

Background: Geometric Deformations via Template-based Image Registration

We first briefly review the concept of template-based deformable image registration (Joshi et al. 2004; Zhang, Singh, and Fletcher 2013), which is widely used to estimate deformable geometric deformations from groupwise images. In this work, we adopt the algorithm of large deformation diffeomorphic metric mapping (LDDMM), which encourages the smoothness of deformation fields and preserves the topological structures of images (Beg et al. 2005).

Given a number of N images $\{I_1, \dots, I_N\}$, the problem of template-based image registration is to find the shortest paths (a.k.a. geodesics) between a template image I and the rest of image data with derived associate deformation fields ϕ_1, \dots, ϕ_N that minimizes the energy function

$$E(I, \phi_n) = \sum_{n=1}^N \frac{1}{\sigma^2} \text{Dist}[I \circ \phi_n(v_n(t)), I_n] + \text{Reg}[\phi_n(v_n(t))], \quad (1)$$

where σ^2 is a noise variance and \circ denotes an interpolation operator that deforms image I with an estimated transformation ϕ_n . The $\text{Dist}[\cdot, \cdot]$ is a distance function that measures the dissimilarity between images, i.e., sum-of-squared differences (Beg et al. 2005), normalized cross correlation (Avants et al. 2008), and mutual information (Wells III et al. 1996). The $\text{Reg}[\cdot]$ is a regularizer that guarantees the smoothness of transformations, i.e.,

$$\begin{aligned} \text{Reg}[\phi_n(v_n(t))] &= \int_0^1 (Lv_n(t), v_n(t)) dt, \\ \text{with } \frac{d\phi_n(t)}{dt} &= -D\phi_n(t) \cdot v_n(t), \end{aligned} \quad (2)$$

where $L : V \rightarrow V^*$ is a symmetric, positive-definite differential operator that maps a tangent vector $v_n(t) \in V$ into its dual space as a momentum vector $m_n(t) \in V^*$. We write $m_n(t) = Lv_n(t)$, or $v_n(t) = Km_n(t)$, with K being an inverse operator of L . The operator D denotes a Jacobian matrix and \cdot represents element-wise matrix multiplication. In this paper, we use a metric of the form $L = -\alpha\Delta + \mathbb{I}$, in which Δ is the discrete Laplacian operator, α is a positive regularity parameter, and \mathbb{I} denotes an identity matrix.

The minimum of Eq. (2) is uniquely determined by solving a Euler-Poincaré differential equation (EPDiff) (Arnold 1966; Miller, Trounev, and Younes 2006) with a given initial condition of velocity fields, noted as $v_n(0)$,

$$\begin{aligned} \frac{\partial v_n(t)}{\partial t} &= -K[(Dv_n(t))^T \cdot m_n(t) + Dm_n(t) \cdot v_n(t) \\ &\quad + m_n(t) \cdot \text{div } v_n(t)], \end{aligned} \quad (3)$$

where the operator D denotes a Jacobian matrix, div is the divergence, and \cdot represents an element-wise matrix multiplication. This is known as the geodesic shooting algorithm (Vialard et al. 2012), which nicely proves that the deformation-based shape descriptor, ϕ_n , can be fully characterized by an initial velocity field, $v_n(0)$.

We are now able to equivalently minimize the energy function in Eq. (1) as

$$\begin{aligned} E(I, v_n(0)) &= \sum_{n=1}^N \frac{1}{\sigma^2} \text{Dist}[I \circ \phi_n(v_n(0)), I_n] \\ &\quad + (Lv_n(0), v_n(0)), \text{ s.t. Eq. (3)}. \end{aligned} \quad (4)$$

For notation simplicity, we will drop the time index in the following sections.

Our Method: MGAug

This section presents a novel algorithm, MGAug, that learns a multimodal latent distribution of geometric transformations represented by the initial velocity fields v_0 . We first introduce a generative model in latent geometric spaces for DA based on VAE, followed by an approximated variational inference. The augmented data is then used to train various image analysis tasks, i.e., image classification or segmentation. Similar to (Zhao et al. 2019; Chen et al. 2022), we employ a joint learning scheme to optimize the MGAug and IAT network parameters. To simplify the notation, we omit the time index of v_0 in the following sections.

Generative Model in Latent Multimodal Geometric Spaces

Given a group of N input images \mathbf{J} with a template I , we assume the latent geometric transformations \mathbf{x} are generated from a number of C clusters. The distribution of \mathbf{x} can be formulated as a Gaussian mixture with means $\boldsymbol{\mu}$ and variances $\boldsymbol{\Sigma}$, specified by a VAE encoder parameterized by β , i.e., $p_\theta(\mathbf{x}|\epsilon)$, where ϵ is a random number generated from $\mathcal{N}(0, \mathbb{I})$. That is to say, the VAE encoder outputs a set of C means $\boldsymbol{\mu}$ and C variances $\boldsymbol{\Sigma}$. A one-hot vector \mathbf{z} is sampled from the mixing probability $\boldsymbol{\pi} \in [0, 1]$ with $\sum_{c=1}^C \pi^c = 1$,

which chooses one component from the Gaussian mixture. In this paper, we set the parameter $\pi = C^{-1}$ to make the variable \mathbf{z} uniformly distributed, which is similar to (Dilokthanakul et al. 2016). The initial velocity field \mathbf{v} is generated from a VAE decoder parameterized by θ and the continuous latent variable \mathbf{x} . The entire process to generate the observed image data \mathbf{J} from a set of latent variables $\{\mathbf{v}, \mathbf{x}, \epsilon, \mathbf{z}\}$ is:

$$\epsilon \sim \mathcal{N}(0, \mathbb{I}), \quad (5)$$

$$\mathbf{z} \sim \text{Mult}(\boldsymbol{\pi}), \quad (6)$$

$$\mathbf{x}|\mathbf{z}, \epsilon \sim \prod_{c=1}^C \mathcal{N}(\boldsymbol{\mu}_{\mathbf{z}_c}(\epsilon, \beta), \boldsymbol{\Sigma}_{\mathbf{z}_c}(\epsilon, \beta))^{\mathbf{z}_c}, \quad (7)$$

$$\mathbf{v}|\mathbf{x} \sim \mathcal{N}(\mathbf{v}_\theta(\mathbf{x}) | 0, \boldsymbol{\Sigma}), \quad (8)$$

$$\mathbf{J}|\mathbf{v}, I, \lambda \sim \mathcal{N}(\mathbf{J} | I \circ \phi(\mathbf{v}), \lambda^2 \mathbb{I}), \quad (9)$$

where $\text{Mult}(\cdot)$ denotes a multinomial distribution, λ^2 is a noise variance in the observed image space, and an identity matrix \mathbb{I} maps a matrix to be diagonal. A graphical representation of our proposed generative model is shown in Fig. 1.

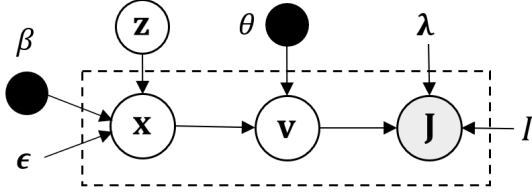


Figure 1: Graphical representation of our proposed generative model in multimodal latent space.

To guarantee the smoothness of the geometric transformations, we define a multivariate Gaussian distribution on the generated initial velocity fields \mathbf{v} in Eq. (8) as

$$p(\mathbf{v}|\mathbf{x}) \propto \exp\left(-\frac{1}{2}(\boldsymbol{\Sigma}^{-1}\mathbf{v}_\theta(\mathbf{x}), \mathbf{v}_\theta(\mathbf{x}))\right). \quad (10)$$

Similar to (Zhang and Fletcher 2013; Zhang, Shao, and Fletcher 2015), we define the covariance matrix $\boldsymbol{\Sigma}$ as an inverse operator of the differential operator, L , which is used in the registration regularity in Eq. (2).

Considering that our input images are measured on a discrete grid, we formulate our image noise model as an i.i.d. Gaussian at each image voxel, i.e.,

$$p(\mathbf{J}|\mathbf{v}, I, \lambda) = \frac{1}{(2\pi)^{M/2}(\lambda)^M} \exp\left(-\frac{\|I \circ \phi(\mathbf{v}) - \mathbf{J}\|_2^2}{2\lambda^2}\right), \quad (11)$$

where M is the total number of image voxels. Putting together Eq. (5) to Eq. (11), we arrive at a generative model

$$p_{\beta, \theta}(\mathbf{J}, \mathbf{v}, \mathbf{x}, \epsilon, \mathbf{z}) = p(\mathbf{J}|\mathbf{v}, I, \lambda) p(\mathbf{v}|\mathbf{x}) p(\mathbf{x}|\mathbf{z}, \epsilon) p(\mathbf{z}) p(\epsilon) \quad (12)$$

Variational Lower Bound

We will train the generative model in Eq. (12) with the variational inference objective, i.e. the log-evidence lower bound

(ELBO). With an assumption that the mean-field variational family $q(\mathbf{v}, \mathbf{x}, \epsilon, \mathbf{z} | \mathbf{J})$ is an approximate to the posterior, we are able to formulate the ELBO as

$$\mathcal{L}_{\text{ELBO}} = \mathbb{E} \left[\log \frac{p_{\beta, \theta}(\mathbf{J}, \mathbf{v}, \mathbf{x}, \epsilon, \mathbf{z})}{q(\mathbf{v}, \mathbf{x}, \epsilon, \mathbf{z} | \mathbf{J})} \right] \quad (13)$$

We factorize the mean-field variational family as $\mathbf{q} = \prod_{i=1}^n q(\mathbf{v}_i | \mathbf{J}_i, I, \lambda) q_{\psi_{\mathbf{x}}}(\mathbf{x}_i | \mathbf{v}_i, \mathbf{J}_i) q_{\psi_{\epsilon}}(\epsilon_i | \mathbf{v}_i) p_{\beta}(\mathbf{z}_i | \mathbf{x}_i, \epsilon_i)$, where i denotes the i -th image. Each variational factor is parameterized with the recognition networks $\psi_{\mathbf{x}}$ and ψ_{ϵ} that output the parameters of the variational Gaussian distributions. Note that we will drop the index i in the following sections for the purpose of notation simplicity.

Using previously defined Eq. (10) and Eq. (11), the posterior $q(\mathbf{v}_i | \mathbf{J}_i, I, \lambda) \propto p(\mathbf{J} | \mathbf{v}, I, \lambda) \cdot p(\mathbf{v} | \mathbf{x})$ is formulated by Baye's rule. Following (Jiang et al. 2016), we can derive the posterior $p_{\beta}(\mathbf{z} | \mathbf{x}, \epsilon)$ as

$$\begin{aligned} p_{\beta}(\mathbf{z}_j = 1 | \mathbf{x}, \epsilon) &= \frac{p(\mathbf{z}_j = 1) p(\mathbf{x} | \mathbf{z}_j = 1, \epsilon)}{\sum_{c=1}^C p(\mathbf{z}_c = 1) p(\mathbf{x} | \mathbf{z}_c = 1, \epsilon)} \\ &= \frac{\pi_j \mathcal{N}(\mathbf{x} | \boldsymbol{\mu}_j(\epsilon; \beta), \boldsymbol{\Sigma}_j(\epsilon; \beta))}{\sum_{c=1}^C \pi_{\mathbf{z}_c} \mathcal{N}(\mathbf{x} | \boldsymbol{\mu}_{\mathbf{z}_c}(\epsilon; \beta), \boldsymbol{\Sigma}_{\mathbf{z}_c}(\epsilon; \beta))}, \end{aligned}$$

where $\mathbf{z}_j, j \in \{1, \dots, C\}$ denotes the j -th element of \mathbf{z} . The variational lower bound can be now formulated as

$$\begin{aligned} \mathcal{L}_{\text{ELBO}} &= \mathbb{E}_{q(\mathbf{x}|\mathbf{J})} [\log P_{\theta}(\mathbf{J}|\mathbf{x})] \\ &\quad - \mathbb{E}_{q(\epsilon|\mathbf{J})} p(\mathbf{z}|\mathbf{x}, \epsilon) [KL(q_{\psi_{\mathbf{x}}}(\mathbf{x}|\mathbf{J}) || p_{\beta}(\mathbf{x}|\epsilon, \mathbf{z}))] \\ &\quad - KL(q_{\psi_{\epsilon}}(\epsilon|\mathbf{J}) || p(\epsilon)) \\ &\quad - \mathbb{E}_{q(\mathbf{x}|\mathbf{J})} q(\epsilon|\mathbf{J}) [KL(p_{\beta}(\mathbf{z}|\mathbf{x}, \epsilon) || p(\mathbf{z}))] \quad (14) \end{aligned}$$

Joint Learning of MAGug With Image Analysis

We demonstrate the effectiveness of MGAug in image analysis tasks (IAT) by developing a joint learning framework. It has been shown in (Zhao et al. 2019; Chen et al. 2022) that these two tasks can be mutually beneficial. The MGAug effectively synthesizes image samples to augment the training dataset, while the IAT can provide extra information on rectifying the learned distributions of latent geometric spaces. An overview of our proposed network architecture is shown in Fig. 2.

Network design of MGAug. MGAug is mainly designed based on the previously introduced inference model, where the approximate posteriors are simulated by neural networks. Analogous to (Kingma and Welling 2013), we let the encoder of MGAug, parameterized by β , approximate the posterior as a mixture of multivariate Gaussians. In the latent space \mathbf{z} , we use non-linear hidden layers to learn the parameters (i.e., means and covariances) of the mixture Gaussians. The decoder, parameterized by θ , outputs augmented velocity fields \mathbf{v}_n , followed by generating their associated deformations ϕ_n (via Eq. (3)) and augmented deformed images. In this paper, we adopt UNet architecture (Ronneberger, Fischer, and Brox 2015) as the network backbone for MGAug. However, other networks such as UNet++ (Zhou et al. 2018) and TransUNet (Chen et al. 2021) can be easily applied.

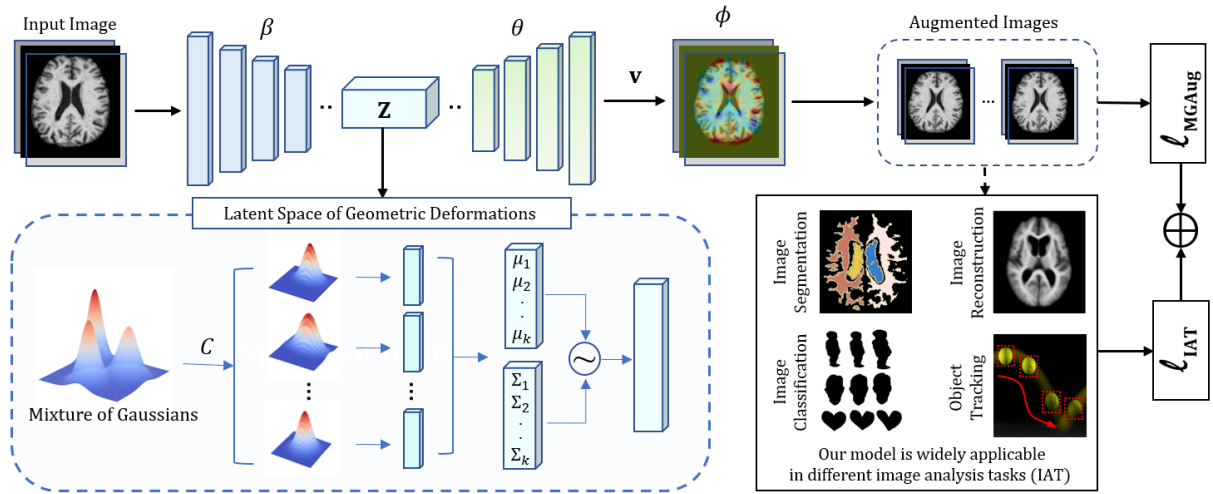


Figure 2: An overview of our model MGAug for image analysis tasks.

Defining $\Theta = (\mathbf{J}, \beta, \theta, \mathbf{x}, \mathbf{z}, \mathbf{v}, \epsilon, I)$ as posterior parameters, we formulate the network loss of MGAug as a combination of dissimilarity between deformed images and templates, a regularity to ensure the smoothness of augmenting transformations, and the variational inference objective as

$$\begin{aligned} \ell_{\text{MGAug}}(\Theta) &= -\log p_{\beta, \theta}(\mathbf{J}, \mathbf{v}, \mathbf{x}, \epsilon, \mathbf{z}) \\ &\approx \frac{\|I \circ \phi(\mathbf{v}(\beta, \theta)) - \mathbf{J}\|_2^2}{2\lambda^2} + \mathcal{L}_{\text{ELBO}} \\ &\quad + \frac{1}{2}(L\mathbf{v}(\beta, \theta), \mathbf{v}(\beta, \theta)) + \text{reg}(\beta, \theta), \end{aligned}$$

where $\text{reg}(\cdot)$ denotes network parameter regularizations.

Network design of IAT. We demonstrate MGAug on the task of image classification and segmentation separately. Other domain-specific tasks, such as image reconstruction, object recognition, and tracking can be integrated similarly.

For classification, assuming we have augmented images (consist of C classes with N_c images per class) and their labels denoted as \hat{y} . The classifier is trained by minimizing the loss

$$\ell_{\text{IAT}}^{\text{clf}} = -\gamma \sum_{n=1}^{N_c} \sum_{c=1}^C \hat{y}_{nc} \cdot \log[y_{nc}(\beta, \theta, w_1)] + \text{reg}(\beta, \theta, w_1), \quad (15)$$

where y_{nc} denotes the predicted label, γ is the weighting parameter, and w_1 is a classification network parameter.

For segmentation, we employ a loss function as a combination of Sørensen–Dice coefficient (Dice 1945) and cross-entropy (CE). Let Q denote the number of segmentation labels, S_q denotes the augmented ground truth, and R_q denotes the prediction with the associated probabilistic map R_q^p for q -th label. We formulate the segmentation loss as

$$\begin{aligned} \ell_{\text{IAT}}^{\text{seg}} &= \tau \sum_{q=1}^Q [1 - \text{Dice}(S_q, R_q(\beta, \theta, w_2))] \\ &\quad + \text{CE}(S_q, R_q^p(\beta, \theta, w_2)) + \text{reg}(\beta, \theta, w_2), \quad (16) \end{aligned}$$

where $\text{Dice}(S_q, R_q) = 2(|S_q \cap |R_q|)/(|S_q| + |R_q|)$ and $\text{CE}(S_q, R_q^p) = -S_q \cdot \log R_q$. The τ is the weighting parameter and w_2 denotes the segmentation network parameters.

The total loss of our joint learning framework of MGAug and IAT is $\ell = \ell_{\text{MGAug}} + \ell_{\text{IAT}}$. We employ an alternative optimization scheme (Nocedal and Wright 1999) to minimize the loss by alternating between the training of the MGAug network and the IAT network without sharing weights, making it an end-to-end network architecture (Zhao et al. 2019; Chen et al. 2022).

Experimental Evaluation

We validate our proposed model, MGAug, on both 2D synthetic datasets and real 3D brain MRI scans, highlighting its effectiveness on training data with limited availability.

Datasets

2D silhouette shapes. We choose Kimia216 (Sebastian, Klein, and Kimia 2004), which is a relatively smaller dataset with seven classes of 2D silhouette shape data (*bone, bottle, children, face, fish, heart, and key*). Each shape class includes approximately 20 binary images, with the size of 28^2 . The total number of our training images for multi-classification is about 140.

2D handwritten digits. We use 70000 handwritten digits of 10 classes (0-9) from the MNIST repository (LeCun 1998). Each class includes approximately 7000 images with the size of 28^2 .

3D brain MRIs. We include 803 subjects of public T1-weighted longitudinal brain MRIs with manually delineated anatomical structures from Open Access Series of Imaging Studies (OASIS) (LaMontagne et al. 2019), Alzheimer’s Disease Neuroimaging Initiative (ADNI) (Jack Jr et al. 2008), Autism Brain Imaging Data Exchange (ABIDE) (Di Martino et al. 2014), and LONI Probabilistic Brain Atlas Individual Subject Data (LPBA40) (Shattuck et al. 2008). Due to the difficulty of

preserving the diffeomorphic property across individual subjects with large age variations, we carefully evaluate images from subjects aged from 60 to 90. All MRIs were pre-processed as $256 \times 256 \times 256$, $1.25mm^3$ isotropic voxels, underwent skull-stripping, intensity normalization, bias field correction and pre-alignment with affine transformations.

Experiments and Implementation Details

We validate the proposed model, MGAug, on both image classification and segmentation tasks. As MGAug falls into the category of transformation-based DA schemes, we mainly focus on comparing its performance with similar baselines: randomly generated affine transformations (ATA, a commonly used augmentation strategy), and two state-of-the-art unimodal generative models based on diffeomorphic registrations (*AdvEigAug* or *AEA*, an augmentation model based on the statistics of a learned latent space of velocity fields (Olut et al. 2020); and *UDA*, a unimodal deformation-based augmentation using random stationary velocity fields (Dalca et al. 2019)).

Evaluation of classification on small datasets. We first validate our model and other baselines on a relatively small dataset of 7-class 2D silhouette shapes. We adopt six classification network backbones, including a three-layer CNN, ResNet18 (He et al. 2016), VGGNet16 (Simonyan and Zisserman 2014), SqueezeNet (Iandola et al. 2016), DenseNet121 (Huang et al. 2017), and Vision Transformer (ViT) (Dosovitskiy et al. 2020).

We carefully determine the optimal number of modes, C , for our multimodal generative model by performing cross-validation with various values of C . The value of C will vary for different image analysis tasks depending on the dataset distributions. For classification, we assume that the value of C is close to the number of classes. Furthermore, we conduct a comprehensive assessment of the augmentation efficiency offered by our proposed approach. This involves augmenting the training dataset to various magnitudes, ranging from 2 to 10 times the size of the original dataset.

To examine the quality of the generated augmenting transformations, we compute the determinant of Jacobian of the deformation fields. Throughout the evaluation process, we employ multiple metrics such as average accuracy (Acc), precision (Prec), and F1-score (F1) to validate the classification performance.

Evaluation of segmentation on real 3D brain MRIs. We validate the performance of all methods on real 3D brain images with a decent size of training data. In this experiment, we employ TransUNet as our network backbone, given its proven superiority in brain segmentation performance (Chen et al. 2021). To ensure a fair comparison of the final segmentation accuracy, we augment the training data three times for all methods, resulting in a total number of approximately 2000 augmented images. We then compare the segmentation dice scores of all augmentation methods over different brain structures.

Evaluation of the quality of augmented images. To further evaluate the quality of the augmented images, we validate MGAug on two relatively large datasets (2D MNIST and 3D brain MRIs) with various levels of reduced training

sample sizes (i.e., 10%, 20%, and 50% of the original size). We augment the training images three times of the original size for all methods.

Parameter setting. We set parameter $\alpha = 3.0$ for the operator L and the number of time steps for Euler integration in EPDiff (Eq. (3)) as 10. We set the noise variance σ as 0.02, the batch size as 16, and use the cosine annealing learning rate scheduler that starts from a learning rate $\eta = 1e^{-3}$ for network training. We run all the models on training and validation images with Adam optimizer until obtaining the best validation performance. The training and prediction procedure of all learning-based methods are performed on a 40GB NVIDIA A100 Tensor Core GPU. For both 2D and 3D datasets, we split the images by using 70% as training, 15% as validation, and 15% as testing images.

Our method is flexible to either automatically estimated or pre-selected template(s) for group-wise data. Therefore, we demonstrate estimated with-in-class template(s) for classification tasks vs. pre-selected templates for segmentation tasks, respectively. In all experiments presented in this paper, we run cross-validation to determine the optimal number of modes C .

Results

The left panel of Fig. 3 reports our model MGAug’s classification accuracy (using ViT as the network backbone) on 2D silhouette shape dataset with different number of modes, C , along with diverse levels of augmented images quantities (i.e., $5\times$, $7\times$, and $10\times$ the original training data size). It suggests that the utilization of a multimodal latent space ($C > 1$) consistently yields superior performance compared to an unimodal distribution ($C = 1$) by more than 2-7%. Our model achieves an optimal performance when $C = 7$, which represents the number of classes in the training data. The right panel of Fig. 3 shows a comprehensive evaluation of classification accuracy across all augmentation methods with an increased number of augmented images in training data. Our method significantly outperforms other baselines by more than 7% of accuracy with different numbers of augmented images. Another interesting observation is that our MGAug achieves comparable classification accuracy when using roughly $3\times$ augmented images for training vs. other baselines using $10\times$ of ground truth images. This indicates the potency of our method in efficiently leveraging augmented data to achieve competitive results.

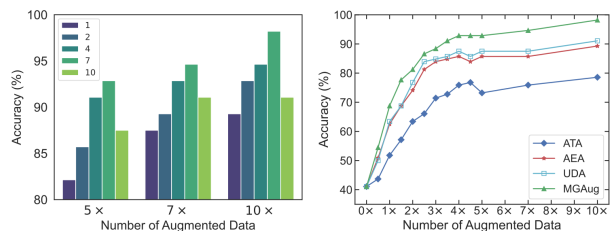


Figure 3: Left: Accuracy comparison on various modes C on 2D shape dataset. Right: A comparison of classification performance for all models over increasing number of augmented data taking all ground truth images.

Table 1: Accuracy comparison on 2D shapes over all models with various network backbones.

	ATA			AEA			UDA			MGAug		
	Acc	Prec	F1	Acc	Prec	F1	Acc	Prec	F1	Acc	Prec	F1
CNN	71.73	73.25	66.89	83.93	88.82	83.07	85.71	87.14	83.73	91.07	92.14	90.78
ResNet18	76.78	79.22	73.44	80.36	82.17	78.76	87.50	90.07	86.83	89.28	90.43	89.15
VGGNet16	73.21	72.46	71.23	85.71	88.04	85.85	85.71	88.57	81.58	89.28	91.21	89.22
SqueezeNet	75.00	75.85	72.99	76.78	79.90	74.53	83.93	87.30	82.73	92.86	93.97	92.59
DenseNet121	75.89	77.54	73.88	87.50	90.79	86.18	89.28	90.86	89.08	94.64	95.55	94.28
ViT	78.57	82.62	76.53	89.28	92.20	89.33	91.07	91.93	96.84	98.21	98.41	98.20

Tab. 1 reports the multi-class classification accuracy on a relatively smaller 2D silhouette shape data across all augmentation methods with various classification network backbones. For a fair comparison, we augment the data $10\times$ of the original training images. MGAug achieves the highest performance, outperforming all baselines by 2-9% of accuracy on six different network backbones.

Fig. 4 visualizes examples of augmented images and the determinant of Jacobian (DetJac) of augmented transformations produced by MGAug. The value of DetJac indicates volume changes when applying augmented deformations on templates. For example, there is no volume change when $\text{DetJac}=1$, while volume shrinks when $\text{DetJac}<1$ and expands when $\text{DetJac}>1$. The value of DetJac smaller than zero indicates an artifact or singularity in the transformation field, i.e., a failure to preserve the diffeomorphic property when the effect of folding and crossing grids occurs. Our method nicely preserves the topological structures of augmented images without introducing artifacts.

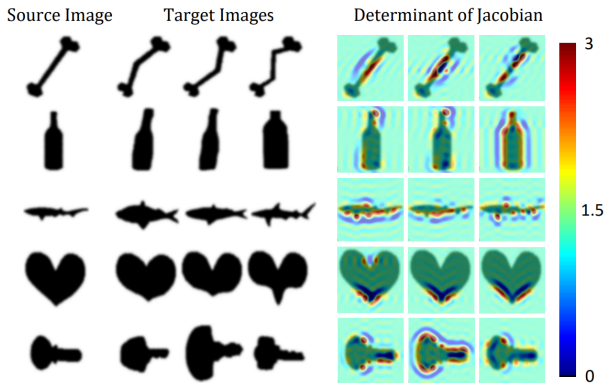


Figure 4: Examples of DetJac generated by MGAug. Left to right: source/template, target images, augmented DetJac overlaid with template images.

Fig. 5 reports the statistics of dice scores (mean and variance) of all augmentation methods over fifteen brain structures experimenting on 30% of training images with 2000 augmented images. Our MGAug outperforms all the baselines with a significant dice improvement in all anatomical structures (at least 2% or higher).

The left panel of Fig. 6 showcases the classification results on the 2D MNIST dataset for all methods, using dif-

ferent percentages of ground truth data during the training phase. Our MGAug method consistently achieves the highest accuracy across all augmentation techniques. Remarkably, MGAug reaches an accuracy of 98.02% (which is the baseline accuracy without any augmentation) using only 20% of the ground truth data, whereas other methods require at least 50% of ground truth data to achieve similar results. Similarly, the right panel of Fig. 6 presents the dice evaluation for 3D brain MRI segmentations, as the percentage of ground truth data used in training is progressively increased. In a manner mirroring the classification results, our MGAug consistently outperforms the baseline algorithms by yielding the highest dice scores. These results indicate that our augmentation method has great potential to better alleviate the heavy need for labor and time-consuming ground-truths.

Additional discussion. It is to our attention that diffusion models have recently become a powerful generative model (Ho, Jain, and Abbeel 2020). In this context, we initiate a preliminary comparison between our MGAug model and data augmentation through a diffusion model operating in the image space (by manipulating image intensities and textures) (Trabucco et al. 2023). This comparison was carried out with a specific focus on classification tasks using the 2D MNIST dataset.

Experimental results show that the diffusion model achieves an accuracy of 97.56% when using 50% of the ground truth labels. This accuracy, interestingly, is slightly lower than what our MGAug method accomplishes (98.02%) when only using 20% of the ground truth data. This may indicate the advantages of multimodal distributions of latent geometric space developed in our model. Our future work will further explore the power of diffusion models in the latent geometric space for efficient data augmentation, which has not been investigated so far.

MGAug vs. intensity-based augmentations. While the primary emphasis of this paper does not fall into the realm of intensity-based augmentations, we compare MGAug with a few notable DA schemes that manipulate image intensities or textures. These methods include *AutoAugment* (Cubuk et al. 2019), *RandAugment* (Cubuk et al. 2020), *AugMix* (Hendrycks et al. 2019), and *TrivialAugment* (Müller and Hutter 2021).

Tab. 2 reports the accuracy comparison of a variety of DA schemes for image classification networks based on the ViT backbone. The testing results on both MNIST digits and 2D

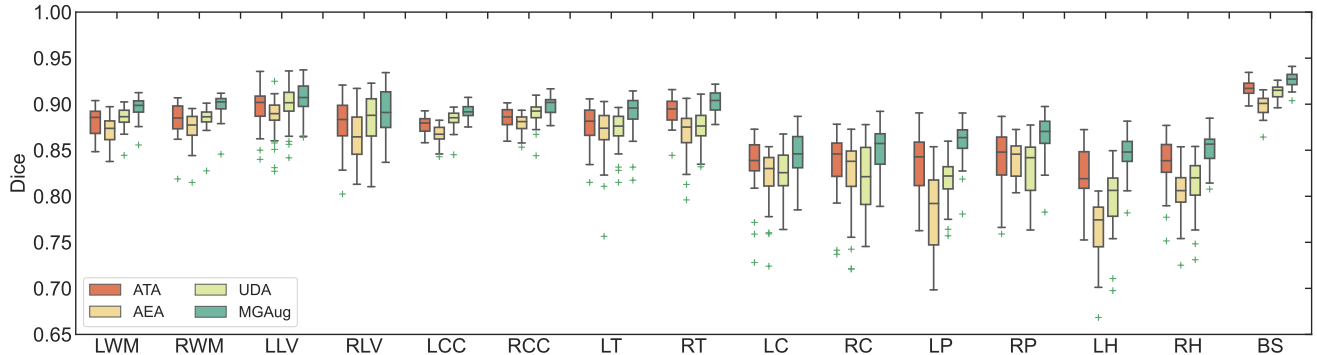


Figure 5: Dice score comparison over fifteen anatomical brain structures, (LWM - Left White Matter, RWM - Right White Matter, LLV - Left Lateral Ventricle, RLV - Right Lateral Ventricle, LCC - Left Cerebellum Cortex, RCC - Right Cerebellum Cortex, LT - Left Thalamus, RT - Right Thalamus, LC - Left Cudate, RC - Right Caudate, LP - Left Putamen, RP - Right Putamen, LH - Left Hippocampus, RH - Right Hippocampus, BS - Brain Stem) for four augmentation methods.

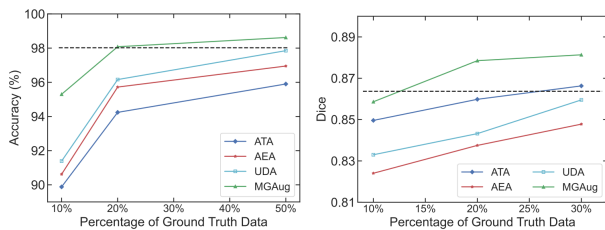


Figure 6: Left to right: classification evaluation on 2D MNIST dataset; segmentation evaluation on 3D brain MRIs with various percentages of ground truth used in the training inference. The horizontal dashed line (- -) serves as a reference, representing the performance achieved when utilizing all available training images without any augmentation.

shape data show that our model consistently outperforms the baselines.

Conclusion & Discussion

In this paper, we present a novel data augmentation model, MGAug, which learns augmenting transformations in a multimodal latent space of geometric deformations reparameterized by low-dimensional tangent spaces of diffeomorphisms. In contrast to existing augmentation models that adopt a unimodal distribution to augment data, our augmentation method fully characterizes the multimodal distribution of image transformations via introducing a mixture of multivariate Gaussians as the prior. Our method significantly improves the performance of multi-class classification (on 2D dataset) and image segmentation (on 3D brain MRIs) and eliminates the artifacts of geometric transformations by preserving topological structures of augmented images. While MGAug focuses on LDDMM, the theoretical tool developed in our model is widely applicable to various registration frameworks, for example, stationary velocity fields (Modat et al. 2012).

To the best of our knowledge, we are the first to learn geometric deformations in a multimodal manner via deep neu-

Table 2: Accuracy comparison on both 2D digits and 2D shape datasets over a mix of augmentation methods (including intensity-based vs. transformation-based DA) on ViT.

Datasets	2D Digits		2D Shape	
	Models	Acc	F1	Acc
AutoAugment	90.82	90.73	76.05	75.25
RandAugment	95.25	95.22	81.25	81.70
AugMix	97.31	97.30	74.28	69.35
TrivialAug	95.48	95.49	83.93	82.75
Affine	95.90	95.84	78.57	76.53
AEA	96.95	96.91	89.28	89.33
UDA	<u>97.85</u>	<u>97.83</u>	<u>91.07</u>	<u>96.84</u>
MGAug	98.62	98.78	98.21	98.20

ral networks. Our augmentation model can be easily applied to different domain-specific tasks, e.g., image reconstruction and object tracking. Interesting future directions based on this work can be i) investigating the model interpretability for classification tasks when geometric deformations are learned in a multimodal manner, and ii) the robustness study of MGAug when image intensity variations occur, i.e., under adversarial noise attacks.

Acknowledgments. This work was supported by NSF CAREER Grant 2239977.

References

- Araslanov, N.; and Roth, S. 2021. Self-supervised augmentation consistency for adapting semantic segmentation. In *Proceedings of the IEEE/CVF Conference on Computer Vision and Pattern Recognition*, 15384–15394.
- Arnold, V. 1966. Sur la géométrie différentielle des groupes de Lie de dimension infinie et ses applications à l’hydrodynamique des fluides parfaits. In *Annales de l’institut Fourier*, volume 16, 319–361.

- Avants, B. B.; Epstein, C. L.; Grossman, M.; and Gee, J. C. 2008. Symmetric diffeomorphic image registration with cross-correlation: evaluating automated labeling of elderly and neurodegenerative brain. *Medical image analysis*, 12(1): 26–41.
- Beg, M. F.; Miller, M. I.; Trounev, A.; and Younes, L. 2005. Computing large deformation metric mappings via geodesic flows of diffeomorphisms. *International journal of computer vision*, 61(2): 139–157.
- Chen, C.; Qin, C.; Ouyang, C.; Li, Z.; Wang, S.; Qiu, H.; Chen, L.; Tarroni, G.; Bai, W.; and Rueckert, D. 2022. Enhancing MR image segmentation with realistic adversarial data augmentation. *Medical Image Analysis*, 82: 102597.
- Chen, J.; Lu, Y.; Yu, Q.; Luo, X.; Adeli, E.; Wang, Y.; Lu, L.; Yuille, A. L.; and Zhou, Y. 2021. Transunet: Transformers make strong encoders for medical image segmentation. *arXiv preprint arXiv:2102.04306*.
- Cubuk, E. D.; Zoph, B.; Mane, D.; Vasudevan, V.; and Le, Q. V. 2019. Autoaugment: Learning augmentation strategies from data. In *Proceedings of the IEEE/CVF Conference on Computer Vision and Pattern Recognition*, 113–123.
- Cubuk, E. D.; Zoph, B.; Shlens, J.; and Le, Q. V. 2020. Randaugment: Practical automated data augmentation with a reduced search space. In *Proceedings of the IEEE/CVF conference on computer vision and pattern recognition workshops*, 702–703.
- Dalca, A. V.; Balakrishnan, G.; Guttag, J.; and Sabuncu, M. R. 2019. Unsupervised learning of probabilistic diffeomorphic registration for images and surfaces. *Medical image analysis*, 57: 226–236.
- Di Martino, A.; Yan, C.-G.; Li, Q.; Denio, E.; Castellanos, F. X.; Alaerts, K.; Anderson, J. S.; Assaf, M.; Bookheimer, S. Y.; Dapretto, M.; et al. 2014. The autism brain imaging data exchange: towards a large-scale evaluation of the intrinsic brain architecture in autism. *Molecular psychiatry*, 19(6): 659–667.
- Dice, L. R. 1945. Measures of the amount of ecologic association between species. *Ecology*, 26(3): 297–302.
- Dilokthanakul, N.; Mediano, P. A.; Garnelo, M.; Lee, M. C.; Salimbeni, H.; Arulkumaran, K.; and Shanahan, M. 2016. Deep unsupervised clustering with gaussian mixture variational autoencoders. *arXiv preprint arXiv:1611.02648*.
- Dosovitskiy, A.; Beyer, L.; Kolesnikov, A.; Weissenborn, D.; Zhai, X.; Unterthiner, T.; Dehghani, M.; Minderer, M.; Heigold, G.; Gelly, S.; et al. 2020. An image is worth 16x16 words: Transformers for image recognition at scale. *arXiv preprint arXiv:2010.11929*.
- Gao, Y.; Tang, Z.; Zhou, M.; and Metaxas, D. 2021. Enabling data diversity: efficient automatic augmentation via regularized adversarial training. In *International Conference on Information Processing in Medical Imaging*, 85–97. Springer.
- Hauberg, S.; Freifeld, O.; Larsen, A. B. L.; Fisher, J.; and Hansen, L. 2016. Dreaming more data: Class-dependent distributions over diffeomorphisms for learned data augmentation. In *Artificial intelligence and statistics*, 342–350. PMLR.
- He, K.; Zhang, X.; Ren, S.; and Sun, J. 2016. Deep residual learning for image recognition. In *Proceedings of the IEEE conference on computer vision and pattern recognition*, 770–778.
- Hendrycks, D.; Mu, N.; Cubuk, E. D.; Zoph, B.; Gilmer, J.; and Lakshminarayanan, B. 2019. Augmix: A simple data processing method to improve robustness and uncertainty. *arXiv preprint arXiv:1912.02781*.
- Ho, J.; Jain, A.; and Abbeel, P. 2020. Denoising diffusion probabilistic models. *Advances in neural information processing systems*, 33: 6840–6851.
- Hossain, T.; Shishir, F. S.; Ashraf, M.; Al Nasim, M. A.; and Shah, F. M. 2019. Brain tumor detection using convolutional neural network. In *2019 1st international conference on advances in science, engineering and robotics technology (ICASERT)*, 1–6. IEEE.
- Huang, G.; Liu, Z.; Van Der Maaten, L.; and Weinberger, K. Q. 2017. Densely connected convolutional networks. In *Proceedings of the IEEE conference on computer vision and pattern recognition*, 4700–4708.
- Iandola, F. N.; Han, S.; Moskewicz, M. W.; Ashraf, K.; Dally, W. J.; and Keutzer, K. 2016. SqueezeNet: AlexNet-level accuracy with 50x fewer parameters and 0.5 MB model size. *arXiv preprint arXiv:1602.07360*.
- Jack Jr, C. R.; Bernstein, M. A.; Fox, N. C.; Thompson, P.; Alexander, G.; Harvey, D.; Borowski, B.; Britson, P. J.; L. Whitwell, J.; Ward, C.; et al. 2008. The Alzheimer’s disease neuroimaging initiative (ADNI): MRI methods. *Journal of Magnetic Resonance Imaging: An Official Journal of the International Society for Magnetic Resonance in Medicine*, 27(4): 685–691.
- Jaderberg, M.; Simonyan, K.; Zisserman, A.; et al. 2015. Spatial transformer networks. *Advances in neural information processing systems*, 28.
- Jayakumar, N.; Hossain, T.; and Zhang, M. 2023. SADIR: Shape-Aware Diffusion Models for 3D Image Reconstruction. In *International Workshop on Shape in Medical Imaging*, 287–300. Springer.
- Jiang, Z.; Zheng, Y.; Tan, H.; Tang, B.; and Zhou, H. 2016. Variational deep embedding: An unsupervised and generative approach to clustering. *arXiv preprint arXiv:1611.05148*.
- Joshi, S.; Davis, B.; Jomier, M.; and Gerig, G. 2004. Unbiased Diffeomorphic Atlas Construction for Computational Anatomy. *NeuroImage*, 23, Supplement 1: 151–160.
- Kim, J.; and Pavlovic, V. 2016. A shape preserving approach for salient object detection using convolutional neural networks. In *Pattern Recognition (ICPR), 2016 23rd International Conference on*, 609–614. IEEE.
- Kingma, D. P.; and Welling, M. 2013. Auto-encoding variational bayes. *arXiv preprint arXiv:1312.6114*.
- Krebs, J.; Delingette, H.; Mailhé, B.; Ayache, N.; and Mansi, T. 2019. Learning a probabilistic model for diffeomorphic registration. *IEEE transactions on medical imaging*, 38(9): 2165–2176.

- Krizhevsky, A.; Sutskever, I.; and Hinton, G. E. 2017. ImageNet classification with deep convolutional neural networks. *Communications of the ACM*, 60(6): 84–90.
- LaMontagne, P. J.; Benzinger, T. L.; Morris, J. C.; Keefe, S.; Hornbeck, R.; Xiong, C.; Grant, E.; Hassenstab, J.; Moulder, K.; Vlassenko, A. G.; et al. 2019. OASIS-3: longitudinal neuroimaging, clinical, and cognitive dataset for normal aging and Alzheimer disease. *MedRxiv*.
- LeCun, Y. 1998. The MNIST database of handwritten digits. <http://yann.lecun.com/exdb/mnist/>.
- Lim, S.; Kim, I.; Kim, T.; Kim, C.; and Kim, S. 2019. Fast autoaugmentation. *Advances in Neural Information Processing Systems*, 32.
- Miller, M. I.; Trounev, A.; and Younes, L. 2006. Geodesic shooting for computational anatomy. *Journal of mathematical imaging and vision*, 24(2): 209–228.
- Mirza, M.; and Osindero, S. 2014. Conditional generative adversarial nets. *arXiv preprint arXiv:1411.1784*.
- Modat, M.; Daga, P.; Cardoso, M. J.; Ourselin, S.; Ridgway, G. R.; and Ashburner, J. 2012. Parametric non-rigid registration using a stationary velocity field. In *2012 IEEE Workshop on Mathematical Methods in Biomedical Image Analysis*, 145–150. IEEE.
- Moreno-Barea, F. J.; Strazzera, F.; Jerez, J. M.; Urda, D.; and Franco, L. 2018. Forward noise adjustment scheme for data augmentation. In *2018 IEEE symposium series on computational intelligence (SSCI)*, 728–734. IEEE.
- Müller, S. G.; and Hutter, F. 2021. Trivialaugument: Tuning-free yet state-of-the-art data augmentation. In *Proceedings of the IEEE/CVF international conference on computer vision*, 774–782.
- Muralikrishnan, S.; Chaudhuri, S.; Aigerman, N.; Kim, V. G.; Fisher, M.; and Mitra, N. J. 2022. GLASS: Geometric latent augmentation for shape spaces. In *Proceedings of the IEEE/CVF Conference on Computer Vision and Pattern Recognition*, 18552–18561.
- Nocedal, J.; and Wright, S. J. 1999. *Numerical optimization*. Springer.
- Olut, S.; Shen, Z.; Xu, Z.; Gerber, S.; and Niethammer, M. 2020. Adversarial data augmentation via deformation statistics. In *European Conference on Computer Vision*, 643–659. Springer.
- Pang, J.; Chen, K.; Shi, J.; Feng, H.; Ouyang, W.; and Lin, D. 2019. Libra r-cnn: Towards balanced learning for object detection. In *Proceedings of the IEEE/CVF conference on computer vision and pattern recognition*, 821–830.
- Ronneberger, O.; Fischer, P.; and Brox, T. 2015. U-net: Convolutional networks for biomedical image segmentation. In *Medical Image Computing and Computer-Assisted Intervention—MICCAI 2015: 18th International Conference, Munich, Germany, October 5-9, 2015, Proceedings, Part III 18*, 234–241. Springer.
- Sebastian, T. B.; Klein, P. N.; and Kimia, B. B. 2004. Recognition of shapes by editing their shock graphs. *IEEE Transactions on pattern analysis and machine intelligence*, 26(5): 550–571.
- Shattuck, D. W.; Mirza, M.; Adisetiyo, V.; Hojatkashani, C.; Salamon, G.; Narr, K. L.; Poldrack, R. A.; Bilder, R. M.; and Toga, A. W. 2008. Construction of a 3D probabilistic atlas of human cortical structures. *Neuroimage*, 39(3): 1064–1080.
- Shen, Z.; Xu, Z.; Olut, S.; and Niethammer, M. 2020. Anatomical data augmentation via fluid-based image registration. In *International Conference on Medical Image Computing and Computer-Assisted Intervention*, 318–328. Springer.
- Simonyan, K.; and Zisserman, A. 2014. Very deep convolutional networks for large-scale image recognition. *arXiv preprint arXiv:1409.1556*.
- Trabucco, B.; Doherty, K.; Gurinas, M.; and Salakhutdinov, R. 2023. Effective data augmentation with diffusion models. *arXiv preprint arXiv:2302.07944*.
- Vialard, F.-X.; Risser, L.; Rueckert, D.; and Cotter, C. J. 2012. Diffeomorphic 3D image registration via geodesic shooting using an efficient adjoint calculation. *International Journal of Computer Vision*, 97(2): 229–241.
- Wang, J.; and Zhang, M. 2022. Geo-SIC: Learning Deformable Geometric Shapes in Deep Image Classifiers. *arXiv preprint arXiv:2210.13704*.
- Wells III, W. M.; Viola, P.; Atsumi, H.; Nakajima, S.; and Kikinis, R. 1996. Multi-modal volume registration by maximization of mutual information. *Medical image analysis*, 1(1): 35–51.
- Yun, S.; Han, D.; Oh, S. J.; Chun, S.; Choe, J.; and Yoo, Y. 2019. Cutmix: Regularization strategy to train strong classifiers with localizable features. In *Proceedings of the IEEE/CVF international conference on computer vision*, 6023–6032.
- Zhang, M.; and Fletcher, T. 2013. Probabilistic principal geodesic analysis. *Advances in neural information processing systems*, 26.
- Zhang, M.; Shao, H.; and Fletcher, P. T. 2015. A mixture model for automatic diffeomorphic multi-atlas building. In *Med. Image Comput. Comput.-Assisted Intervention Workshop-BAMBI*.
- Zhang, M.; Singh, N.; and Fletcher, P. T. 2013. Bayesian estimation of regularization and atlas building in diffeomorphic image registration. In *International conference on information processing in medical imaging*, 37–48. Springer.
- Zhao, A.; Balakrishnan, G.; Durand, F.; Guttag, J. V.; and Dalca, A. V. 2019. Data augmentation using learned transformations for one-shot medical image segmentation. In *Proceedings of the IEEE/CVF conference on computer vision and pattern recognition*, 8543–8553.
- Zhou, Z.; Rahman Siddiquee, M. M.; Tajbakhsh, N.; and Liang, J. 2018. Unet++: A nested u-net architecture for medical image segmentation. In *Deep learning in medical image analysis and multimodal learning for clinical decision support*, 3–11. Springer.
- Zoph, B.; Cubuk, E. D.; Ghiasi, G.; Lin, T.-Y.; Shlens, J.; and Le, Q. V. 2020. Learning data augmentation strategies for object detection. In *European conference on computer vision*, 566–583. Springer.